
This manuscript has been submitted for publication in GEOLOGY. Please note that subsequent versions of this manuscript may have different content. Please feel free to contact any of the authors; we welcome feedback

----

EXTRUSION DYNAMICS OF DEEP-WATER VOLCANOES REVEALED BY 3D SEISMIC DATA

Qiliang Sun[1,2,3], Christopher A.L. Jackson[4], Craig Magee[4], and Xinong Xie[1,3]

[1]Key Laboratory of Tectonics and Petroleum Resources, China University of Geosciences (Wuhan), Ministry of Education, Wuhan 430074, China

[2]Laboratory for Marine Mineral Resources, Qingdao National Laboratory for Marine Science and Technology, Qingdao 266061, China

[3]College of Marine Science and Technology, China University of Geosciences (Wuhan), Wuhan, Hubei 430074, PR China

[4]Basins Research Group (BRG), Department of Earth Science & Engineering, Imperial College, London, SW7 2BP, UK

Abstract

Submarine volcanism accounts for c. 75% of the Earth's volcanic activity. However, due to difficulties with imaging their exteriors and interiors, deep-water volcanoes are poorly understood in terms of their extrusion dynamics and growth. Here, we use high-resolution 3-D reflection seismic data from the South China Sea to investigate the geometry, distribution, plumbing system, and extrusion dynamics of several Late Miocene-Quaternary, deep-water volcanoes. We show these volcanoes extruded lava flows feeding lobate lava fans, with the former associated with lava tubes emplaced at shallow depths within wet, unconsolidated, near-seafloor sediments. Moreover, we show that 50-97% of the erupted volume is preserved in these long run-out (>9 km) lava flows and not within the volcanic edifice itself. Estimates of erupted lava volumes, which are critical for calculating melt generation and storage conditions, may therefore be erroneous if based solely on edifice mapping, with 3D seismic reflection data allowing more accurate constraints to be placed on the way in which eruption products are spatially partitioned.

Keywords

Volcanism, lava flow channel, lava fan, lava tube, sill, South China Sea

Introduction

The external morphology of volcanoes and their eruptive products reflects, and provides insight into, the processes controlling magma extrusion and volcano construction. By extracting high-resolution, quantitative data on the morphology of volcanic edifcaes (and that of the surrounding lava field) from airborne/shuttle radar topography (e.g. Somoza et al., 2017; Grosse and Kervyn, 2018), and multibeam bathymetry (e.g. Cocchi et al., 2016; Allen et al., 2018), we can calculate melt volume and reconstruct volcano growth. More specifically, the volume of material contained within a volcanic edifice is typically considered equivalent to the total erupted volume, a parameter required to infer melt and storage conditions (e.g. Smith, 1988; Somoza et al., 2017; Grosse and Kervyn, 2018). Whilst these data types capture the external morphology of volcanoes and lava flows, they do not however image their basal surface or internal architecture. Without access to the full 3D structure of these extrusive systems, it is difficult or, in many cases, impossible to test volcano and lava flow growth models, or calculate the volume of erupted mateiral. Several studies have, however, demonstrated that seismic reflection data can be used to map the external morphology, internal architecture, and plumbing system of buried volcanoes in 3D (e.g. Planke et al., 2000; Calvès et al., 2011; Jackson, 2012; Magee et al., 2013; Reynolds et al., 2017). To date, the majority of these studies have focused on those formed in sub-aerial or shallow-marine environments (e.g. Planke et al., 2000; Jackson, 2012; Magee et al., 2013; Reynolds et al., 2018); deep-water volcanoes are still poorly documented and thus understood.

In this study, we use high-resolution 3D seismic reflection data to examine Late Miocene-Quaternary submarine volcanoes emplaced in deep-water (>1.6 km) on highly stretched continental lithosphere in the northern South China Sea (Fig. 1). Based on interpretation of volcano and lava flow structure, distribution, and scale, we discuss emplacement processes, relating our findings to studies of deep-water volcanoes using bathymetry and ROV data. We show that volcano and lava field morphology are are controlled by the nature of deep-water sedimentary setting (e.g. high hydrostatic pressure, unconsolidated seafloor sediments, and slope dips), and that the volcano edifices themselves may comprise only a small part of the total erupted magma volume.

Geological setting

The study area is located on the northern continental slope of the South China Sea (Fig. 1a) (e.g. Briais et al., 1993). Rifting here occurred during the Cretaceous-Early Oligocene, and was superceded by a period of post-rift thermal subsidence in the Late Oligocene-to-Early Miocene (e.g. Ru and Pigott, 1986). Post-rift volcanoes were emplaced both onshore and offshore, with the latter extruded onto continental slope sedimentary rocks in water depths of <300 m (Yan et al., 2006). Cores show these relatively shallow-water volcanoes are composed of basalt, dacite, and rhyolitic tuff (Li and Liang, 1994). Here, we analyze several likely Late Miocene-Quaternary volcanoes, located further basinward of the shallow-water volcanoes, close to the Continent-Ocean Boundary (COB), in an area characterized by current water depths of 1970-2680 m and a mean, broadly southward dip of >1º. Data from nearby ODP sites 1145, 1146, and 1148 reveal that, since the Middle Miocene, sedimentation in the study area has likely been dominated by deposition of a deep-marine (>1.6 km water depth), nanofossil-bearing clay ('soft' seabed) (Wang et al., 2000; Clift et al., 2001); these observations strongly suggest the Late Miocene-Quarternary volcanoes were emplaced in a deep-water setting.

Data and Methods

We use a pre-stack time-migrated 3D seismic reflection survey covering ~350 km^2 (Fig. 1b). Bin spacing is 25 m, and the seismic data have a dominant frequency in the interval of interest of ~40 Hz. We calculate a vertical resolution ($\lambda/4$) of ~10 m for sedimentary rocks and 19-25 m for volcanic materials, assuming seismic velocities of 1540 m/s for the sedimentary strata (based on nearby ODP Site 1146 data; Fig. 1) (Sun et al., 2017) and 3000-4000 m/s for volcanic materials (Text S1). The top and base of volcanic materials can be confidently identified or 'resolved' when thicker than the vertical resolution (i.e. 19-25 m), but can be 'detected' if thicker than the estimated detection limit ($\lambda/8$, 10-13 m). We interpreted six seismic surfaces, correlated to ODP Site 1146, which is located ~65 km west of the study area (Sun et al., 2017): T0 (~2.58 Ma); T1 (~5.3 Ma); TRa (~6.5 Ma); TRb (~8.2 Ma), and TM and BM, which correspond to the top and base of erupted material, respectively.

Observations

We identify three conspicuous seismic facies: (1) conical-shaped features capped by a high-amplitude reflection, and, internally, only weakly to moderately reflective (Figs. 2a, 3c); (2) ribbon-like, broadly strata-concordant, high-amplitude reflections, which emenate from the conical anomalies (Figs. 2a-2b, 3c); and (3) saucer-shaped, strata-discordant, high-amplitude reflections, which underlie the two anomaly types described above (Fig. S2a). Based on their geometry, seismic expression, and development next to the COB, we interpret these features as (1) volcanic edifaces, (2) lava flows, and (3) sills (e.g. Planke et al., 2000; Thomson and Hutton, 2004; Calvès et al., 2011; Jackson et al., 2012). Thirteen volcano edifices and four sill complexes are observed in the 3D survey; for the purposes of this study, we focus on two volcano edifices (V1 and V2) that are large and particularly well-imaged, and considered representative of other structures within the study area (Figs. 2-3).

Volcano edifice 1 (V1) and associated lava flows

V1 is a prominent conical structure covering ~7.2 km^2, with a volume of ~0.82±0.12 km^3, and an average flank dip of ~13.2±1.8° (Fig. 2; Table S1). Where continuous reflections occur within V1, they lie sub-parallel to its flanks, and converge down-dip towards the surface BM, onto which they downlap (Fig. 2a). V1 is onlapped by overlying reflections, with the oldest onlapping reflection correlating to TRa (~6.5 Ma); this suggests V1 is latest Miocene-earliest Pliocene (Fig. 2d). A downward-tapering, sub-vertical zone of chaotic seismic reflections underlie V1 (Fig. 2d).

V1 is surrounded by an asymmetric apron of moderate-to-high amplitude reflections that extend up to 1.5 km from the main edifice, and which are up to 202±29 m thick (Figs. 2c-d) (Table S3). A package of moderate-to-very high-amplitude reflections extend another c. 1.5 km downdip of this apron (Figs 1b, 2c). In detail, the latter package contains very high-amplitude, channel-like geometries that terminate downdip into or are flanked at prominent bends by, moderate-amplitude, fan-like geometries; we interpret these two features as lava flow channels (C1-C3) and fans (F1-F4), respectively (Fig. 2). The lava flow channels are sinuous, <340 m wide, and usually bisect the lava fans (Figs 2c-d). Together, lava flow-related features (i.e. apron, channels, and fans) emanating from V1 cover an area of ~14 km^2 (Tables S2-S3), have an average thickness of ~57.2±7.9 m, and thus have a volume of ~0.81±0.12 km^3; this volume is ~99% of the volume of V1 (~0.82±0.12 km^3) and ~50% of the total erupted volume.

Volcano edifice 2 (V2) and associated lava flows

V2 is elliptical in plan-view, with a long and short axis of ~1.2 km and ~0.6 km, respectively (Fig. 3a-b). Its flanks dip 26.4±3.3° and it is smaller than V1, covering only ~0.44 km^2 (volume of 0.02-0.03 km^3) (Fig. 3a; Table S1). Its top is of moderate amplitude and is irregular, with the oldest onlapping reflections correlating to T1 (~5.3 Ma); this suggests V2, like V1, is latest Miocene-earliest Pliocene. Reflections within V2 are chaotic, and, similar to V1, V2 is underlain by a vertical zone of disturbance (Fig. 4a). V2 lacks a lava apron, instead being directly flanked by relatively straight, up to 9.2 km long lava flow channels on its south-eastern side (C4-C7) (Fig. 3a). Lava flow C6 is unusual in that underlying strata are truncated at the base of the flow, defining 'ramps' that are up to ~56.8±7.9 m high and that dip at ~23.5±3.0° (Figs. 3d-e1). Beyond the main ramp (Fig. 3b), the lava flows thickens to 226.7±32.1 m, where it is defined by stacked, high-amplitude reflections that have a lobate geometry in plan-view (F5) (Figs. 3a, 3c, 3e-e1). At its distal end, the pinchout of F5 is defined by abutment against another basal ramp (Figs. 3e-e1). F5 is then capped by a younger, sill-fed lava fan (F6) (Figs. 3e-e1, Text S2). The V2-sourced lava flows (C4-C7 and F5) cover ~11.5 km^2 (~4.20 km^2 of lava flow channels and ~7.32 km^2 of lava fan). Given the average thickness of the lava flow channels (~52.5±7.5 m) and fans (~94.5±13.5 m), we calculate the total volume of V2-sourced lava flows to be 0.92±0.13 km^3; this value is ~37 times greater than the volume of the V2 volcano itself (0.025±0.005 km^3), representing ~97% of the total erupted volume.

Discussion

Volume balance of volcano edifice and lava flow

High-resolution 3D seismic data allow us to calculate the volumes of material contained within volcano edifices and in flanking lava flows. We show that most (i.e. 50-97%) of the erupted material is transported away from the imaged volcanoes, an observation comparable to that made for subaerial fall deposits (Pyle, 1989), and silica-rich, deep-ocean volcanic eruptions (Carey et al., 2018). Importantly, we show that the flanking lava flows in particular do not have concordant bases, but can instead erode into underlying sediment during extrusion (Fig. 3c); accurately calculating their volume therefore requires an understanding of the basal morphology of the lava flows, as well as flow thickness. Our results therefore suggest that erupted magma volume estimates based solely on remote sensing of the seabed may be incorrect (e.g. Robinson and Eakins, 2006). More specifically, we argue that, due to an inability to accurately map the thickness and extent of the lava field using these data, we may underestimate the total erupted magma volumes, thereby compromising our understanding of total melt volume and storage conditions, eruption rates, eruption durations, and associated risk assessments (e.g. Stevens et al., 1999; Arnulf et al., 2014). Difficulties with mapping the near-vent volume of erupted material are compounded by the fact that erupted material may be transported a long distance (i.e. >10 km) from the source volcano (e.g. Gregg and Fornari, 1998).

Deep-water eruption dynamics

We show that volcanoes are typically either flanked by an asymmetric lava apron, which is broader on their downslope (SE) side, or lava flow channels that flowed south-eastwards (Figs. 2a, c-d, 3a). These observations suggest local slope, of only a few degrees (c. 1°), controls the direction of lava flow, with those fed by particularly voluminous eruptions able to flow several tens of kilometres (e.g. C5 and C6; Figs. 2c, 3a). Similar to subaerial volcanoes, high eruption rates and low magma viscosities may generate long run-out flows (e.g. Cashman et al., 1999). However, long run-out lava flows are rarer in submarine environments due to relatively rapid cooling and hardening of magma upon contact with seawater (e.g. Holcomb et al., 1988). We propose that, in addition to eruption onto a slope, the formation of lava tubes ("the conduit beneath the surface of solidified lava through which molten lava flows"; Greeley, (1987)) was a fundamental control on lava run-out distance. We suggest lava tubes would have formed as magma flowed downslope, with hardening of its surface and formation of a solidified crust preventing further heat loss within the tube core. Moreover, the crystallization of magma would release latent heat, which could, to some extent, compensate for the heat lost via surficial cooling (Miles and Cartwright, 2010).

Extrusion into relatively deep water (i.e. a few kilometres) may also have played a role in driving the formation of long run-out lava flows. At these depths, the high hydrostatic pressure (>16 Mpa) would have inhibited degassing and fragmentation, causing the lava to maintain its low viscosity and to flow further (Gregg and Fornari, 1998). Lava flow run-out may also have been facilitated by the gravitational force of lava flow itself, and sustained pressure from newly erupting lava emanating from the source volcano.

Lava flow eventually ceased in distal areas due to gradual cooling and crystallization of the erupted melt (Cashman et al., 1999). We suggest that, in the case of the straight lava flows (C5 and 6), lava transported from within the axial tube would temporarily accumulate at the transient end of the flow, possibly forming a magma pool (Greeley, 1987). Lava entering the tube from the ongoing volcanic eruption would cause an increase in pressure, with the cooled and crytallised material at the flow toe forming a transient impermeable barrier. Eventually, pressure buildup would be sufficient to rupture this frontal barrier, leading to emplacement of a fan downdip of the frontmost base-lava ramp (F5; Fig. 3a, c-d1) (Griffiths, 2000). However, in the case of fans (e.g. F1-4) fed by sinuous channels (Figs. 2c-d), we suggest these were emplaced in a process similar to that documented by Miles and Cartwright (2010), with lobate lava flow fed and bisected by a ‘lava tube’ through magma inflation. At the end of sinuous lava flow channels (e.g. C1), the main channel bifurcated to form a lobate fan (F3, Figs. 2c-d), which was also probably caused by flow branching triggered by magma cooling (Griffiths, 2000).

Finally, the overall geometry and internal architecture of the imaged lava flows indicate substrate rheology was a key control on emplacement dynamics. For example, the base-lava ramps suggest these flows were able to eroded down into the seabed, likely because the pre-eruption substrate was cold, wet, and unconsolidated. We suggest that, by being denser, the lava flow was able to sink down into or 'dredge' the soft sediments (Duffield et al., 1986), with the high temperatures also permitting thermal erosion of substrate by intra-flow turbulance (Griffiths, 2000).

Conclusions

High-resolution 3-D seismic data allow us to image and map the internal structure, and to better understand the extrusion dynamics of, and to calculate the total amount of material erupted from, a suite of deep-water volcanoes; such insights cannot readily be gained from analysis of remote sensing data. High hydrostatic pressure, an inclined seabed, and low-strength, very fine-grained, near-seabed sediments, combined with formation of lava tubes and extrusion of low-viscocity magmas, are likely responsible for anomalously long-distance lava run-out in this deep-water environment. Moreover, we show that a large amount (as high as ~97%) of the erupted materials are transported away from the volcano edifices, suggesting that volume of deep-water volcanic edifices may not faithfully archive eruption size or magma production. Considering the deep-water conditions (e.g. inclined slope and unconsolidated sediments) in the study area are common elsewhere, the conclusions derived from this study can be probably used in other deep-water sedimentary basins and some mid-ocean ridges.

Acknowledgment

This work was supported by the National Scientific Foundation of China (Grant Nos. 91528301, 41676051 and 41372112), the Programme of Introducing Talents of Discipline to Universities (No. B14031) and the Fundamental Research Funds for the Central Universities-the China University of Geosciences (Wuhan) (No. CUG160604). We thank the China National Offshore Oil Company for permission to release the data. Dr. Rebecca Bell is thanked for generously providing office space during the visit of Qiliang Sun to Imperial College.

References

Allen, R.W., Berry, C., Henstock, T.J., Collier, J.S., Dondin, F.J-Y., Rietbrock, A., Latchman, J.L., and Robertson, R.E.A., 2018, 30 Years in the Life of an Active Submarine Volcano: A Time - Lapse Bathymetry Study of the Kick-'em-Jenny Volcano, Lesser Antilles: Geochemistry, Geophysics, Geosystems, v. 19, p. 715-731, doi: doi.org/10.1002/2017GC007270.

Arnulf, A.F., Harding, A.J., Kent, G.M., Carbotte, S.M., Canales, J.P., and Nedimović, M.R., 2014, Anatomy of an active submarine volcano: Geology, v. 42, p. 655-658, doi: 10.1130/G35629.1.

Briais, A., Patriat, P., and Tapponnier, P., 1993, Updated interpretation of magnetic anomalies and seafloor spreading stages in the South China Sea: Implications for the Tertiary tectonics of Southeast Asia: Journal of Geophysical Research, v. 98, p. 6299-6328, doi:10.1029/92JB02280.

Calvès, G., Schwab, A.M., Huuse, M., Clift, P.D., Gaina, C., Jolley, D., Tabrez, A.R., and Inam, A., 2011, Seismic volcanostratigraphy of the western Indian rifted margin: The pre-Deccan igneous province: Journal of Geophysical Research, v. 116, p. B01101, doi: 10.1029/2010JB000862.

Carey, R., Soule, S.A., Manga, M., White, J.D.L., McPhie, J., Wysoczanski, R., Jutzeler, M., Tani, K., Yoerger, D., Fornari, D., Caratori-Tontini, F., Houghton, B., Mitchell, S., Ikegami, F., Conway, C., Murch, A., Fauria, K., Jones, M., Cahalan, R., and McKenzie, W., 2018. The largest deep-ocean silicic volcanic eruption of the past century: Science Advances, v. 4, p. e1701121, doi: 10.1126/sciadv.1701121.

Cashman, K.V., Thornber, C.R., and Kauahikaua, J.P., 1999, Cooling and crystallization of lava in open channels, and the transition of pahoehoe lava to `a`a: Bulletin of Volcanology, v. 61, p. 306-323, doi: 10.1007/s004450050.

Clift, P.D., Lin, J., and ODP Leg 184 Scientific Party, 2001, Patterns of extension and magmatism along the continent-ocean boundary, South China margin: Geological Society, London, Special Publications, v. 187, p. 489-510, doi: 10.1144/GSL.SP.2001.187.01.24.

Cocchi, L., Masetti, G., Muccini, F., and Carmisciano, C., 2016, Geophysical mapping of Vercelli Seamount: Implications for Miocene evolution of the Tyrrhenian back arc basin: Geoscience Frontiers, v. 7, p. 835-849, doi: 10.1016/j.gsf.2015.06.006.

Duffield, W.A., Bacon, C.R., and Delaney, P.T., 1986, Deformation of poorly consolidated sediment during shallow emplacement of a basalt sill, Coso Range, California: Bulletin of Volcanology, v. 48, p. 97-107, doi: 10.1007/BF01046545.

Grosse, P., and Kervyn, M., 2018, Morphometry of terrestrial shield volcanoes: Geomorphology, v. 304, p. 1-14, doi: 10.1016/j.geomorph.2017.12.017.

Greeley, R., 1987, The role of lava tubes in Hawaiian volcanoes, U.S. Geological Survey Professional Paper 1350, p. 1589-1602.

Gregg, T.K.P., and Fornari, D.J., 1998, Long submraine lava flows: Observations and results from numerical modeling: Journal of Geophysical Research, v. 103, p. 27517-27531, doi: 10.1029/98JB02465.

Griffiths, R.W., 2000, The Dynamics of lava flows: Annual Review of Fluid Mechanics, v. 32, p. 477-518, doi: 10.1146/annurev.fluid.32.1.477.

Holcomb, R.T., Moore, J.G., Lipman, P.W., and Belderson, R.H., 1988, Voluminous submarine lava flows from Hawaiian volcanoes: Geology, v. 16, p. 400-404, doi: 10.1130/0091-7613(1988)016<0400:VSlava flow fanH>2.3.CO;2.

Jackson, C.A.-L., 2012, Seismic reflection imaging and controls on the preservation of ancient sill-fed magmatic vents: Journal of the Geological Society, London: v. 169, p. 503-506, doi: 10.1144/0016-76492011-147.

Li, P., and Liang, H., 1994. Cenozoic magmatism in the Pearl River Mouth Basin and its relationship to the basin evolution and petroleum accumulation: Guangdong Geology, v. 9, p. 23-34 (in Chinese with English abstract).

Magee, C., Hunt-Stewart, E., and Jackson, C.A.-L., 2013, Volcano growth mechanisms and the role of sub-volcanic intrusions: Insights from 2D seismic reflection data. Earth and Planetary Science Letters, v. 373, p. 41-53, doi: 10.1016/j.epsl.2013.04.041.

Miles, A., and Cartwright, J., 2010, Hybrid fl ow sills: A new mode of igneous sheet intrusion: Geology, v. 38, p. 343-346, doi: 10.1130/G30414.1.

Planke, S., Symonds, P., Alvestad, E., and Skogseid, J., 2000, Seismic volcanostratigraphy of large-volume basaltic extrusive complexes on rifted margins: Journal of Geophysical Research, v. 105, p. 19335-19351, doi: 10.1029/1999JB900005.

Pyle, D.M., 1989. The thickness, volume and grainsize of tephra fall deposits: Bulletin of Volcanology, v. 51, p. 1-15, doi: 10.1007/BF01086757.

Reynolds, P., Holford, S., Schofield, N., and Ross, A., 2017, Three-dimensional seismic imaging of ancient submarine lava flows: an example from the southern Australian margin: Geochemistry, Geophysics, Geosystems, v. 18, p. 3840-3853, doi: 10.1002/2017GC007178.

Reynolds, P., Schofield, N., Brown, R.J. and Holford, S.P., 2018, The architecture of submarine monogenetic volcanoes-insights from 3D seismic data: Basin Research, v. 30, p. 437-451, doi: 10.1111/bre.12230.

Robinson, J.E., and Eakins, B.W., 2006, Calculated volumes of individual shield volcanoes at the young end of the Hawaiian Ridge: Journal of Vocanology and Geothermal Research, v. 151, p. 309-617, doi: 10.1016/j.jvolgeores.2005.07.033.

Ru, K., and Pigott, J.D., 1986, Episodic rifting and subsidence in the South China Sea: AAPG Bulletin, v. 70, p. 1136-1155.

Somoza, L., Gonzalez, F.J., Barker, S.J., Madureira, P., Medialdea, T., de Ignacio, C., Lourenco, N., Leon, R., Vazquez, J.T., and Palomino, D., 2017. Evolution of submarine eruptive activity during the 2011-2012 El Hierro event as documented by hydroacoustic images and remotely operated vehicle observations: Geochemistry, Geophysics, Geosystems, v. 18, p. 3109-3137, doi: 10.1002/2016GC006733.

Stevens, N.F., Wadge, G., and Murray, J.B., 1999, Lava flow volume and morphology from digitised contour maps: a case study at Mount Etna, Sicily: Geomorphology, v. 28, p. 251-261, doi: 10.1016/S0169-555X(98)00115-9.

Sun, Q.L., Xie, X.N., Piper, D.J.W., Wu, J., and Wu, S.G., 2017, Three dimensional seismic anatomy of multi-stage mass transport deposits in the Pearl River Mouth Basin, northern South China Sea: Their ages and kinematics: Marine Geology, v. 393, p. 93-108, doi: 10.1016/j.margeo.2017.05.005.

Thomson, K., and Hutton, D., 2004, Geometry and growth of sill complexes: Insights using 3-D seismic from the North Rockall Trough: Bulletin of Volcanology, v. 66, p. 364–375, doi: 10.1007/s00445-003-0320-z.

Wang, P., Prell, W.L., and ODP 184 scientists., 2000, Proceedings of the Ocean Drilling Program, Initial Reports, 184. Ocean Drilling Program, College Station, TX 2000.

Yan, P., Deng, H., Liu, H.L., Zhang, Z., and Jiang, Y., 2006, The temporal and spatial distribution of volcanism in the South China Sea region: Journal of Asian Earth Sciences, v. 27, p. 647-659, doi: 10.1016/j.jseaes.2005.06.005.

Yang, S., Qiu, Y., and Zhu, B., 2015, Atlas of Geology and Geophysics of the South China Sea: China Navigation Publications, Tianjin.

Figure Captions

Figure 1: Geological setting of the study area. (a) Bottom left: regional setting of the South China

Sea that is bounded by the Red River Strike-slip faults (RRFs) to the west and by the subduction trench (Manila Trench) to the east. The study area (marked with red square) is located to the south of Dongsha Islands. ODP sites 1145, 1146 and 1148 are labeled. The base map is modified from Yang et al. (2015); (b) Seabed morphologies of the study area. Distributions of volcano edifices (red), sills (blue), lava flows (green) and locations of Figures 2c and 3a are labeled. The contour lines are in 100 ms (twt).

Figure 2: Seismic characteristics of deep-water volcano (V1) and associated lava flow channels/fans. (a) Seismic profile crosscuts the volcano edifice and associated lava flow; (b) Seismic profile crosscuts the lava flow (enhanced seismic anomalies); (c) and (d) RMS amplitude map (± 30 ms along the surface BM) and its interpretations. Volcanic apron, lava flow channels/fans are labeled. See Figure S1 for the un-interpreted version of this profile.

Figure 3: Seismic characteristics of lava flow channels/fans fed by V2) and S1/S2. (a) and (b) Variance slice (extracted from the surface BM) and its interpretations; (c) Seismic profile crosscuts V2 and along lava flow channel (C6) and Lava fans (F5 and F6). The V2 has a sharp boundary to the upslope. See Figure S1 for the un-interpreted version of this profile; (d) and (d1) Enlargement of the end of lava flow channel (ramp structure) and its line drawings; (e) and (e1) Enlargement and its line drawings of the lava fans (F5 and F6).

Figure 1

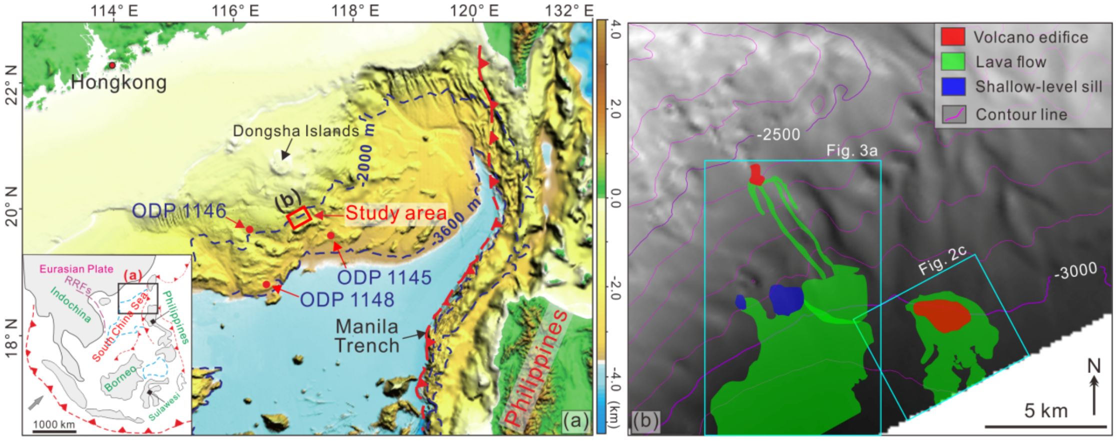
114° E
116° E
118° E
120° E
132° E
22° N
20° N
18° N
Hongkong
Dongsha Islands
-2000 m
(b)
ODP 1146
Study area
-3600 m
ODP 1145
ODP 1148
Manila Trench
Philippines
Eurasian Plate
(a)
RRFs
Indochina
South China Sea
Philippines
Borneo
Sulawesi
1000 km
4.0
2.0
0.0
-2.0
-4.0 (km)
(a)
Volcano edifice
Lava flow
Shallow-level sill
Contour line
-2500
Fig. 3a
Fig. 2c
-3000
N
5 km
(b)

Figure 2

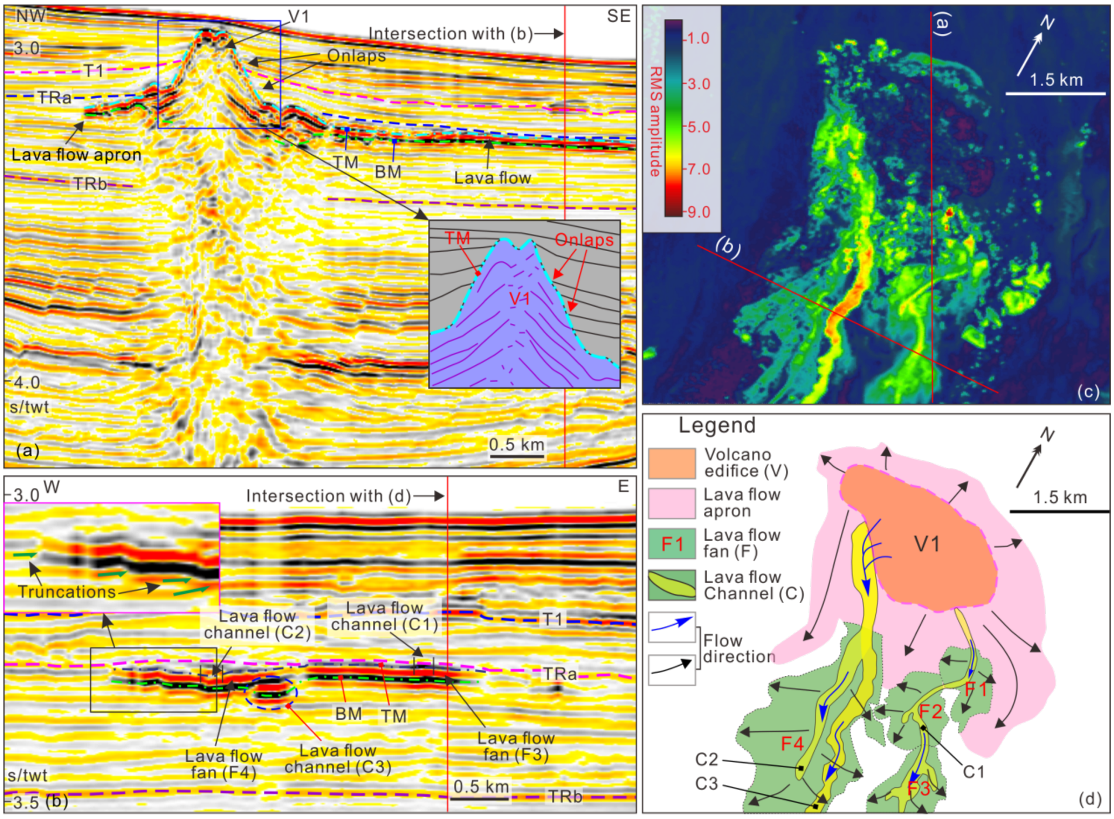

NW
SE
V1
Intersection with (b)
Onlaps
3.0
T1
TRa
Lava flow apron
TM
BM
Lava flow
TRb
TM
Onlaps
V1
4.0
s/twt
(a)
0.5 km
RMS amplitude
-1.0
-3.0
-5.0
-7.0
-9.0
(a)
N
1.5 km
(b)
(c)
3.0
W
E
Intersection with (d)
Truncations
Lava flow channel (C2)
Lava flow channel (C1)
T1
TRa
BM
TM
Lava flow fan (F4)
Lava flow channel (C3)
Lava flow fan (F3)
s/twt
0.5 km
3.5
(b)
TRb
Legend
Volcano edifice (V)
Lava flow apron
Lava flow fan (F)
Lava flow Channel (C)
Flow direction
N
1.5 km
V1
F1
F2
F3
F4
C1
C2
C3
(d)

Figure 3

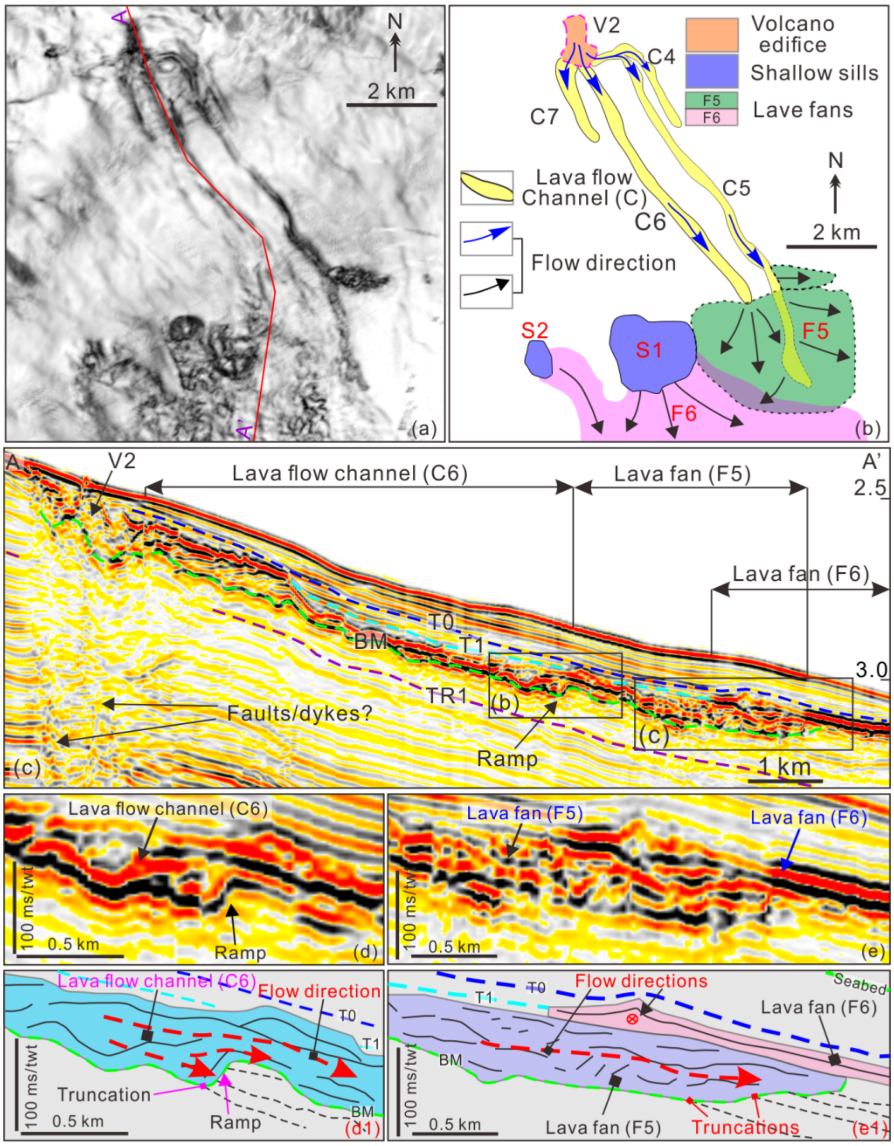

N
2 km
(a)
V2
C4
C7
C5
C6
Volcano edifice
Shallow sills
F5
F6
Lave fans
Lava flow Channel (C)
Flow direction
N
2 km
S2
S1
F5
F6
(b)
A
V2
Lava flow channel (C6)
Lava fan (F5)
A'
2.5
Lava fan (F6)
T0
T1
BM
3.0
TR1
(b)
Faults/dykes?
(c)
Ramp
1 km
(c)
Lava flow channel (C6)
100 ms/twt
0.5 km
Ramp
(d)
Lava fan (F5)
Lava fan (F6)
100 ms/twt
0.5 km
(e)
Lava flow channel (C6)
Flow direction
T0
T1
100 ms/twt
Truncation
0.5 km
Ramp
BM
(d1)
T0
T1
Flow directions
Seabed
Lava fan (F6)
BM
100 ms/twt
0.5 km
Lava fan (F5)
Truncations
(e1)

Supplementary materials

Supplementary Text

Text S1: Seismic velocities of volcanic materials

Seismic velocities of offshore volcanoes and mafic sills have been demonstrated by a few studies and they are greatly variable. These volcanoes and sills intersected by boreholes offshore western India and offshore Norway show that the seismic velocities range from 3300 to 5500 m/s (Calvès et al., 2011) and 4500 to 7400 m/s (Berndt et al., 2000), respectively. From the 'pull-up' seismic reflections, Magee et al. (2013) indicated that the seismic velocities of volcanoes offshore southern Australia were from 2365 to 6739 m/s with an average velocity of 4000 m/s. While Reynolds et al. (2018) shown that the seismic velocities of submarine volcanoes were between 2200 and 4025 m/s in the Bass Basin. Recent studies suggested that the submarine volcano eruptions consisted of a lot of pumices (Carey et al., 2018; Manga et al., 2018) which probably have lower seismic velocities than the denser deep-seated sills. Besides, layered structures within the volcano edifices like those documented by Magee et al. (2013) and Reynolds et al. (2018) are observed in this study. Therefore, we infer that the seismic velocities in this study are probably similar to the referred two cases above and their average velocities of 3000-4000 m/s are used in this study.

Text S2: Shallow sills and sheeted lava flows

South of V2, we map two areally extensive, partly merged lava flows emanating from the upper tips of inclined sheets fringing saucer-shaped sills (i.e. S1 and S2). Moreover, a few linear structures rooting from the joints of sills and feeding the lava fan (F6) are also observed (Fig. S2a). F6 is directly onlapped by surface T0 and underlain by F5 (Figs. 3c, 3e-e1). A narrow, vertical seismic chaotic/blanking zone directly occurred underneath the saucer-shaped sills (Fig. S2a). Similar to other lava fans, F6 is also characterized by a single positive high-amplitude seismic event (Fig. S2a). It extends beyond the seismic coverage and it is much bigger than other lava fans in the study area (Fig. S2a; Table S3). Unlike the volcano edifices which usually had only one main vent, the sills probably had many pathways to transport igneous materials to the paleo-seabed (Fig. S2a). This fissure-like eruption maybe lead to the larger covering area and quite constant thickness of lava fan 6 (F6) (Fig. 3c, S2a).

Supplementary tables

Table S1: Dimensions of volcano edifices. [a]diameter and dip are average values.

Volcano edifice	[a]Diameter/m	Height/m	Area/km^2	Volume/km^3	[a]Dip/°
Volcano edifice 1 (V1)	3018	353.5±50.5	7.15	0.820±0.120	13.2±1.8
Volcano edifice 1 (V2)	714	177.5±25.5	0.44	0.025±0.005	26.4±3.3

Table S2: Dimensions of lava flow channels (C). Please not that all the lengths of lava flow channels are measured along their axes. [a]maximum lengths (including the inferred part of lava flow channels); [b]minimum length (C3 extends beyond the 3D survey); [c]thickneses cannot be measured, because of lava flow channels (C1 and C2) are only identified on the plan-view map (RMS and variance slice map); [d]area and volume don't include the inferred part of C5.

Lava flow channels		Length/km	Width/m	Thickness/m	Area/km^2	Volume/km^3
Volcano edifices 1-related	C1	2.86[a]	55-273	unknown[c]	0.31[a]	unknown[c]
	C2	3.66[a]	94-340	unknown[c]	0.56[a]	unknown[c]
	C3	4.60[b]	163-340	46.0±6.0	0.84[a]	0.039±0.005
Volcano edifices 2-related	C4	2.80	172-229	52.5±7.5	0.54	0.028±0.004
	C5	9.15[a]	185-267	56.0±8.0	1.52[d]	0.085±0.012[d]
	C6	6.39	203-285	54.0±6.0	1.47	0.079±0.009
	C7	1.93	236-427	49.5±6.5	0.67	0.033±0.004

Table S3: Dimensions of lava flow fans and lava flow apron. [a]Diameter is calculated from the area as a circle. [b]Minimum areas and volumes, because of limited data coverage. C = Lava flow channel; S = Sill; V = Volcano edifice.

Lava flow fans	Diameter/m	Area/km^2	Thickness/m	Volume/km^3	Feeder	Shape
Lava flow fan 1 (F1)	944[a]	0.70	34.5±5.5	0.024±0.004	C1	Lobate
Lava flow fan 2 (F2)	1050[a]	0.87	34.5±5.5	0.030±0.005	C1	Lobate
Lava flow fan 3 (F3)	997[a]	0.78[b]	34.5±5.5	0.027±0.004[b]	C1	Lobate
Lava flow fan 4 (F4)	2171[a]	3.70[b]	34.5±5.5	0.128±0.020[b]	C2	Lobate
Lava flow fan 5 (F5)	3054[a]	7.32	94.5±13.5	0.692±0.099	C5/C6	Lobate
Lava flow fan 6 (F6)	7906[a]	49.07[b]	47.5±6.5	2.331±0.319[b]	S1/S2	Lobate
Lava flow apron	3182[a]	7.95	70.0±10.0	0.557±0.080	V1	Ring

Supplementary figures

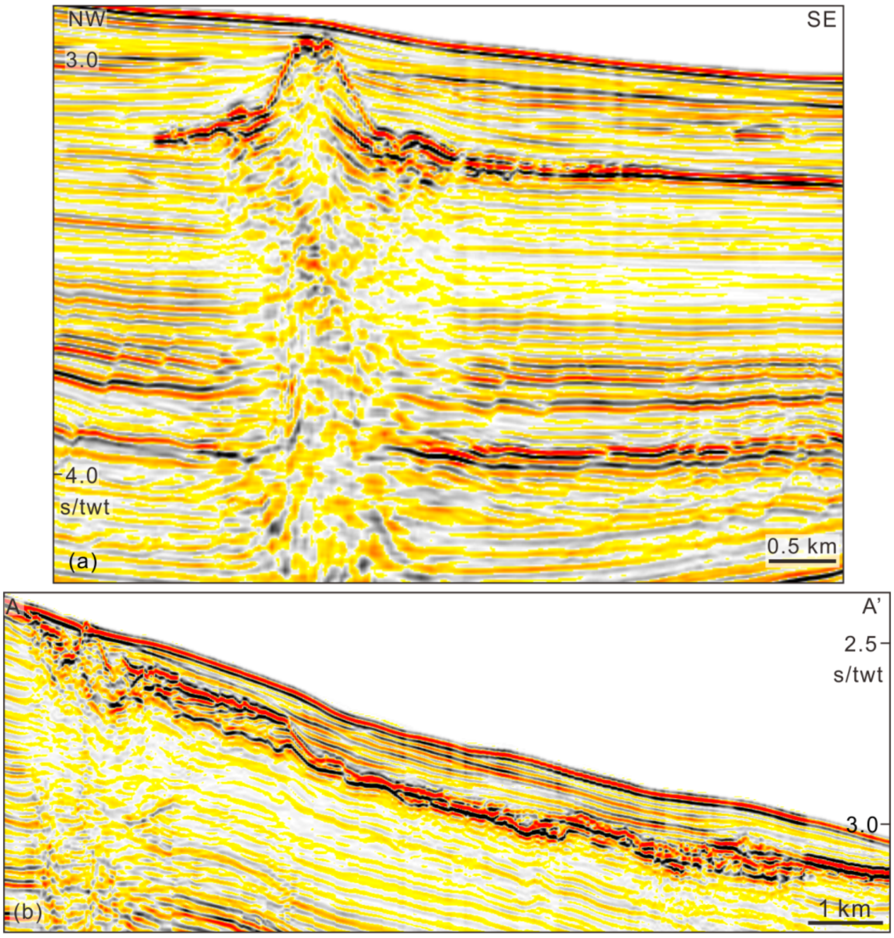

Figure S1: (a) Un-interpreted version of Figure 2a; (b) Un-interpreted version of Figure 3c. The figures are zero-phase and displayed with the Society of Exploration Geophysicists (SEG) normal polarity, whereby a downward increase in acoustic impedance corresponds to a positive (red) reflection.

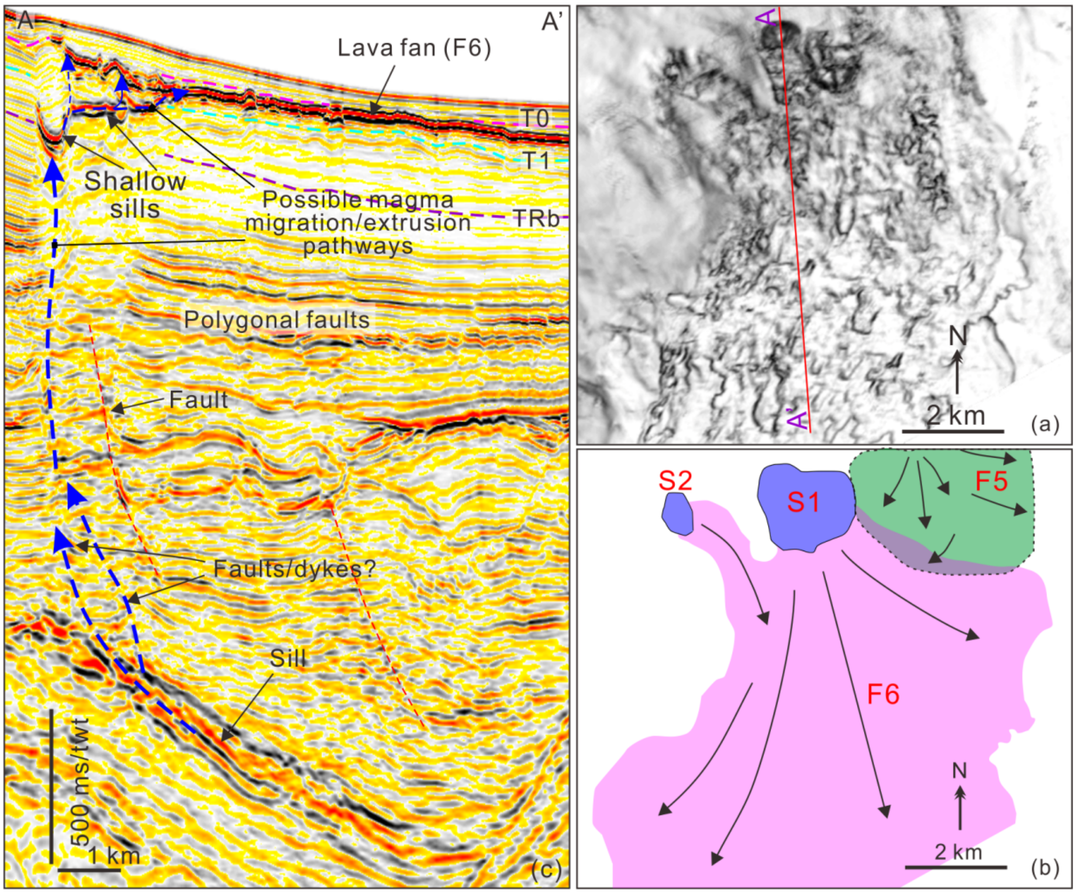

Figure S2: Seismic characteristics of lava flow fan (F6) fed by S1 and S2. (a) and (b) Variance slice (extracted from the surface BM) and its interpretations; (c) Seismic profile shows magma pluming system from deep-seated sill, shallow sills and lava fan. S = sill.

References

Berndt, C., Skogly, O.P., Planke, S., Eldholm, O., and Mjelde, R., 2000, High-velocity break up-related sills in the Vøring Basin, off Norway. Journal of Geophysical Research-Solid Earth, v. 105, p. 28443-28454, doi: 10.1029/2000JB900217

Calvès, G., Schwab, A.M., Huuse, M., Clift, P.D., Gaina, C., Jolley, D., Tabrez, A.R., and Inam, A., 2011, Seismic volcanostratigraphy of the western Indian rifted margin: The pre-Deccan igneous province: Journal of Geophysical Research, v. 116, p. B01101, doi: 10.1029/2010JB000862.

Carey, R., Soule, S.A., Manga, M., White, J.D.L., McPhie, J., Wysoczanski, R., Jutzeler, M., Tani, K., Yoerger, D., Fornari, D., Caratori-Tontini, F., Houghton, B., Mitchell, S., Ikegami, F., Conway, C., Murch, A., Fauria, K., Jones, M., Cahalan, R., and McKenzie, W., 2018, The largest deep-ocean silicic volcanic eruption of the past century: Science Advances, v. 4, p. e1701121, doi: 10.1126/sciadv.1701121.

Magee, C., Hunt-Stewart, E., and Jackson, C.A.-L., 2013, Volcano growth mechanisms and the role of sub-volcanic intrusions: Insights from 2D seismic reflection data: Earth and Planetary Science Letters, v. 373, p. 41-53, doi: 10.1016/j.epsl.2013.04.041.

Manga, M., Fauria, K.E., Lin, C., Mitchell, S.J., Jones, M., Conway, C.E., Degruyter, W., Hosseini, B., Carey, R., Cahalan, R., Houghton, B.F., White, J.D.L., Jutzeler, M., Soule, S.A., and Tani, K., 2018, The pumice raft-forming 2012 Havre submarine eruption was effusive: Earth and Planetary Science Letters, v. 489, p. 49-58, doi: 10.1016/j.epsl.2018.02.025.

Reynolds, P., Schofield, N., Brown R.J., and Holford, S.P., 2018, The architecture of submarine monogenetic volcanoes - insights from 3D seismic data: Basin Research, v. 30, p. 437-451, doi: 10.1111/bre.12230.